

Radiative decay of optically excited coherent plasmons in a two-dimensional electron gas

M. Voßbünger, H. G. Roskos,* F. Wolter, C. Waschke, and H. Kurz

Institut für Halbleitertechnik II, Rheinisch-Westfälische Technische Hochschule Aachen, Sommerfeldstrasse 24, D-52056 Aachen, Germany

K. Hirakawa, I. Wilke, and K. Yamanaka

Institute of Industrial Science, University of Tokyo, 7-22-1 Roppongi, Minato-ku, Tokyo 106, Japan

Received July 21, 1995; revised manuscript received December 7, 1995

We report on the observation of coherent submillimeter-wave emission from optically excited plasmons in a two-dimensional electron gas. Phase-synchronous plasma oscillations are induced by femtosecond optical pulses generating electron-hole pairs in the accumulation channel of an AlGaAs/GaAs heterostructure. The radiative decay of the grating-coupled plasmons is traced in time by terahertz-emission spectroscopy. An analysis of the data suggests that ultrafast thermalization and current surges are the plasmon-driving mechanism. © 1996 Optical Society of America

1. INTRODUCTION

The radiative decay of grating-coupled plasmons in a two-dimensional (2D) electron gas in semiconductor heterostructures is an interesting candidate for a solid-state terahertz- (THz-) radiation source. With an appropriate sample design, the emission frequency of this emitter is tunable over a wide range by variation of the carrier density in the 2D electron gas (2DEG).¹ To date, only quasi-static far-infrared (FIR) emission studies based on electrical-current-induced plasma oscillations at AlGaAs/GaAs and SiO₂/Si heterointerfaces have been performed.²⁻⁵ Other experiments have focused on the absorption of cw FIR radiation⁶⁻⁸ or on the nonlinear optical properties of plasmons in Raman measurements.⁹ The emission properties of impulsively excited nonequilibrium plasma oscillations, however, have not been studied yet. In this paper we present the first detailed report on the observation of electromagnetic-wave emission from 2D plasma oscillations at an AlGaAs/GaAs interface driven by femtosecond optical pulses. We detect the THz radiation by time-domain THz-emission spectroscopy, a technique permitting the selective measurement of coherent (i.e., phase-synchronous) FIR radiation phenomena in the frequency range from 0 to 4 THz.¹⁰⁻¹² Here we present measurements of the emission characteristics as a function of sample temperature, excitation density, optical polarization, and photon energy. The data permit a detailed discussion of both the excitation mechanism and the signal decay processes.

2. TWO-DIMENSIONAL PLASMONS AT HETEROINTERFACES

The sample consists of a heterostructure formed by an intrinsic GaAs layer and a 57-nm-thick selectively doped Al_{0.3}Ga_{0.7}As layer (7 nm of undoped Al_{0.3}Ga_{0.7}As at the

interface, 50 nm of Al_{0.3}Ga_{0.7}As doped with Si on top). All the layers are grown by molecular beam epitaxy on a semi-insulating GaAs substrate. At the wafer surface, 5 nm of GaAs is deposited to prevent oxidation of Al in the Al_{0.3}Ga_{0.7}As layer underneath. A metal grating on top of the sample consists of 50-nm-thick Al lines with a period d of 3 μm and a ratio $r = 0.75$ between linewidth and grating period. The grating permits both excitation of the 2DEG by FIR electromagnetic radiation and emission of radiation from the 2DEG. Without the grating, the 2DEG does not couple directly to FIR electromagnetic radiation.

Electrons from the dopants in the Al_{0.3}Ga_{0.7}As layer are transferred to the lower-band-gap GaAs underneath. By Coulomb interaction with the localized dopant ions, the electrons accumulate at the heterointerface and form a 2DEG with a density N_s of $5.4 \times 10^{11} \text{ cm}^{-2}$ and a low-temperature mobility of $4 \times 10^5 \text{ cm}^2/(\text{V s})$, both measured by magnetotransport measurements.¹³ The band bending by the spatially separated charges is illustrated in Fig. 1, showing the results of a self-consistent band-diagram calculation published in Ref. 14 for parameters very close to those of our sample. In the confining field of 70 kV/cm, a 10-nm-wide quantized accumulation channel is formed at the AlGaAs/GaAs interface. The lowest (second) electronic energy eigenstate E_0 (E_1) is located 50 meV (70 meV) above the edge of the conduction band at the interface. The low-temperature quasi-Fermi energy is 18 meV above the E_0 and is still below E_1 . Hence, at cryogenic temperatures, only the first eigenstate is occupied by electrons. With regard to optical excitation of electron-hole pairs, we point out that only electrons, but not holes, are confined at the interface.

Collective excitation leads to plasma oscillations of the 2DEG. The grating imposes a strict propagation direction on the plasmons, permitting only wave vectors oriented perpendicular to the grating lines. Plas-

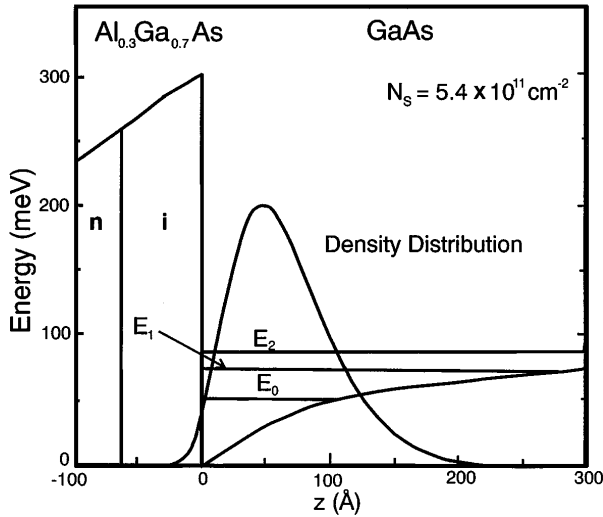


Fig. 1. Self-consistently calculated band diagram at the heterointerface of the sample, with data taken from Ref. 14.

mon propagation under other angles is suppressed, as no electric-field components parallel to the grating can exist under the influence of screening by the grating. The plasmon frequency ω_{pl} is given in the long-wavelength limit ($k_F \gg k_{||} \gg \omega_{THz}/c$) and in local approximation by¹⁵

$$\omega_{pl}^2 = \frac{N_s e^2}{2m^* \epsilon_0 \bar{\epsilon}} k_{||}, \quad (1)$$

where m^* is the effective electron mass in the 2DEG and $\bar{\epsilon}$ denotes the effective dielectric constant. $\bar{\epsilon}$ reflects both the dielectric screening by the semiconductor and the influence of the metal grating. The plasmon wave vector $k_{||}$ can assume only discrete values^{16–18}:

$$k_{||} = \frac{2\pi n}{d}. \quad (2)$$

$n = 1, 2, 3, \dots$ is the order of the harmonics of the spatial charge-density modulation imposed by the grating.

In the plasmon dispersion, forbidden gaps appear at wave vectors with values that are multiples of π/d . The widths of the gaps are determined by the screening efficiency of the grating.¹⁹ Furthermore, the plasmon dispersion for each order n is split into two branches with a radically different coupling to FIR electromagnetic waves for normal incidence or emission.²⁰ One branch consists of modes that interact with electromagnetic radiation. These radiative plasmon modes are characterized by nonequilibrium charge-density distributions with an inversion symmetry relative to the center of the open regions of the grating. The nonequilibrium charge distribution of the plasmon branch that does not couple to radiation is symmetric across the regions between the grating lines. For the same wave vector, the frequency of radiative modes is lower than that of nonradiative modes, which reflects the more effective screening of the plasma oscillations by the grating metallization.¹⁶

Under oblique incidence or emission, the coupling of nonradiative modes to FIR radiation is no longer strictly forbidden.²⁰ Still, the coupling efficiency of the radiative modes is at least $40\times$ stronger than that of the nonradiative modes for all the incidence or emission angles.

When radiative and nonradiative modes are equally excited, the FIR emission is dominated by radiative modes for all the emission angles.

The effective dielectric constant $\bar{\epsilon}$ of the radiative modes can be approximated for large values of r by an expression derived for fully metallized surfaces. In this so-called covered-surface limit, $\bar{\epsilon}$ is given by^{16,21}

$$\bar{\epsilon} = \frac{\epsilon_2 + \epsilon_1 \coth(k_{||}D)}{2}. \quad (3)$$

D denotes the thickness of the layer separating the 2DEG from the grating ($D = 62$ nm, including the 5-nm-thick GaAs cap layer). ϵ_1 is the dielectric constant of AlGaAs; ϵ_2 , that of GaAs [$\epsilon_1 = 11.7$, $\epsilon_2 = 12.4$ (Ref. 22)]. For the parameters of the sample ($m^* = 0.071 m_0$), we estimate the frequencies of the radiative plasmon modes to be 0.35, 0.66, 0.93, and 1.18 THz for $n = 1, 2, 3, 4$, respectively. With a surface coverage of $r = 0.75$ of our grating coupler, the covered-surface approximation does not strictly hold anymore. A nonanalytical but rigorous calculation of the conductivity tensor with a nonperturbative model²³ yields higher emission frequencies: 0.47, 0.90, 1.25, and 1.40 THz, for $n = 1, 2, 3, 4$, respectively.

3. EXPERIMENTS

For the time-resolved detection of coherent electromagnetic radiation from impulsively excited plasmons, we utilize a THz-emission-spectroscopy setup such as that illustrated in Fig. 2(a). The sample is excited by 100-fs optical pulses (20-meV FWHM bandwidth) from a Ti:sapphire laser. The optical beam strikes the sample under an angle θ_{in} of 45° . The size of the excited spot is $0.5\text{--}1$ mm². THz radiation, emitted in the direction of the reflected optical beam, is collected by off-axis paraboloidal mirrors and is detected with a photoconductive dipole an-

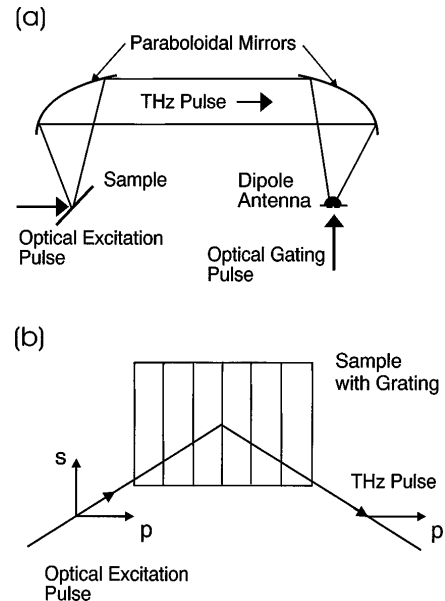


Fig. 2. (a) Setup for the time-resolved detection of optically excited coherent THz radiation from plasmons in a 2DEG. (b) View of the sample with the grating lines. The directions and the polarizations of the optical excitation beam and the generated THz radiation are shown.

tenna gated by a time-delayed portion of the excitation beam.^{10–12}

Figure 2(b) displays the polarizations of the optical and the THz beams with respect to the grating lines for the measurements described below. The lines of the grating are oriented perpendicular to the plane of incidence.²⁴ Except for the measurements given in Subsection 4.A, the optical excitation beam is *p* polarized (electrical-field vector of the optical beam parallel to the plane of incidence). In Subsection 4.A the polarization is varied between *s* and *p* polarization. As expected from the orientation of the plasma oscillations, the polarization of the detected THz radiation is perpendicular to the grating lines; radiation polarized parallel to the grating lines is not observed in the experiments.

The angle of THz-wave emission is defined by the phase (wave front) of the optical pump beam.^{12,25} Coherent emission occurs in the forward and the backward directions, along the reflected and the transmitted optical beams (provided that the refractive indices for the optical and the THz beams are equal). The grating period d of $3\ \mu\text{m}$ is too small to select an emission direction for radiation with a frequency in the 1-THz regime (with 1 THz corresponding to a free-space wavelength of $300\ \mu\text{m}$) by means of constructive and destructive interference.²⁶

Nevertheless, the grating affects the THz-emission direction in a more subtle way, by diffraction of the optical excitation beam. With 333 lines/mm, one calculates backward-diffraction angles θ_{out} of 11.25° , 26.8° , 45° , and 74.4° for orders $m = -2, -1, 0, +1$, respectively, from the grating equation, $\sin(\theta_{\text{out}}) - \sin(\theta_{\text{in}}) = m\lambda/d$. Experimentally, we indeed observe reflected optical beams in all these directions. In the forward direction the optical radiation experiences diffraction in the same way. As a consequence, the 2DEG is excited by multiple (> 2) optical beams rather than by a single one. These beams are not separated in space because the plasma is excited in the near field of the grating. However, the wavelets of what is to develop into separate far-field beams already carry the phase information that distinguishes the diffracted beams from one another. This phase (or timing) difference is transferred to the phase of the coherent plasma oscillations of the 2DEG on excitation. One expects to detect emission of coherent THz radiation along each forward- and backward-diffracted optical beam. Indeed, emission into the $m = -2, -1, 0, +1$ backward directions is observed in the experiments (the forward directions were not studied in this respect). The THz-radiation cones of the different orders overlap resulting in a continuous intensity-modulated signal spread over a wide angle. The temporal characteristics of the radiation do not vary significantly with the direction of emission. We therefore concentrate below on the characteristics of the most intense beam of coherent THz radiation, that emitted in the direction of the $m = 0$ reflected optical beam ($\theta_{\text{out}} = 45^\circ$).

4. RESULTS

A. Low-Temperature Emission from Plasmons

Figure 3 presents results of measurements performed at a sample temperature of 8 K. The sample is excited optically with an average pump power of 80 mW. At the

photon energy of 1.590 eV, charge carriers in the GaAs layer are generated. The density of electron–hole pairs photogenerated directly in the accumulation layer is $1 \times 10^{10}\ \text{cm}^{-2}$ at an excitation power of 80 mW. The photoinduced carrier density remains smaller than the doping-related background plasma density of $5 \times 10^{11}\ \text{cm}^{-2}$. Accumulation effects, to be expected if the recombination time constant of the electron–hole pairs would exceed the 13-ns laser pulse-repetition period, are not observed.

The upper part of Fig. 3 displays the temporal waveforms of the detected coherent THz radiation for different polarizations of the optical excitation beam (*s* and *p* polarizations). A THz signal consisting of several oscillations is observed. The asymmetric shape is a first indication that the signal is composed of several contributions with different frequencies. The smaller oscillations beginning 5.5 ps after the onset of the main signal result from reflections at the wafer's back side. A THz pulse propagating into the substrate and reflected at the back side overlaps with the main signal emitted directly into free space. The waveform of the main signal does not change significantly with the polarization of the excitation beam.

The lower part of Fig. 3 shows the Fourier transforms of the time-domain data. For the Fourier analysis, the reflection in the time-domain data is numerically cut off (temporal windowing). The Fourier spectra are not corrected for the spectral characteristics of the detection system that peaks at 1 THz and rolls off to a cutoff above 3 THz.^{12,25} The THz-emission spectra shown in Fig. 3 reveal emission maxima at 0.5, 0.9, and 1.3 THz. The peak positions coincide well with the plasmon resonances calculated above for orders $n = 1, 2, 3$, respectively. They are also in good agreement with the plasmon frequencies obtained in quasi-static THz-emission experiments based on current-induced plasma oscillations.³ This is strong evidence that the THz signal observed in our experiments re-

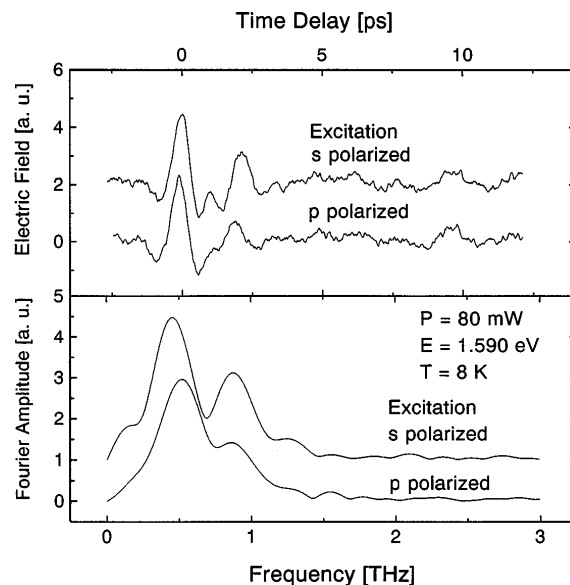


Fig. 3. Low-temperature THz-wave emission from optically excited plasmons. Both the time-domain data and their Fourier transforms are displayed for the two polarizations of the optical beam. The plane of incidence is oriented perpendicular to the lines of the grating coupler.

sults from plasma oscillations in the 2DEG because of the lateral intrasubband polarization in the lowest subband of the accumulation layer. Intersubband transitions, as an additional possible reason for FIR-light emission, can be excluded. The frequency of the lowest possible intersubband transition $[(E_1 - E_0)/h = 4.9 \text{ THz}]$ is beyond the experimental accessible range. The coupling of the 2D plasmons with LO phonons can be neglected because of the high frequency of the LO phonons ($\nu_{\text{LO}} = 8.8 \text{ THz}$) in GaAs. As THz-emission spectroscopy is sensitive only to coherent phenomena, the plasma oscillation modes must be phase locked, with the phase being determined by the ultrashort optical excitation pulse.

The spectrum of the THz radiation does not change significantly with the polarization of the light pulses as one would expect if plasmon generation were an effect associated with the electrical-field vector of the optical beam. The small differences between the peak frequencies for the two polarization directions are artifacts of the spectral windowing prior to Fourier transformation. The insensitivity with respect to the polarization of the optical beam is a clear indication that the excitation of the plasmons occurs by a scalar process such as deposition of energy into the plasma and/or photogeneration of carriers. The small change in amplitude is explained by the polarization dependence of the optical reflection coefficient of the grating. This anisotropy may also be responsible for the better-pronounced plasmon features for s-polarized excitation.

B. Dependence on Photon Energy

Low-temperature THz-emission experiments are performed at different photon energies of the pump beam. Figure 4 shows the time-domain data; Fig. 5, their Fourier transforms. The average power of the pump beam is kept constant while the photon energy (wavelength) is varied. Both the waveform and the spectrum of the emitted THz radiation remain independent of the photon energy of the pump pulse, but the amplitude of the THz radiation changes significantly. For excitation below the low-temperature band gap of GaAs (1.515 eV), no THz emission is detected at all. Only for excitation above the band gap is emission observed. The amplitude of the emitted signal rises continuously with the photon energy until the highest photon energy used in this experiment (1.614 eV) is reached.

It is obvious from the data shown in Figs. 4 and 5 that plasmon excitation does not occur directly by intraband (free-carrier) absorption. The excitation of coherent plasmons is related, rather, to interband (valence-to-conduction-band) optical excitation leading to electron-hole-pair generation. In Fig. 6 the photon-energy dependence of the Fourier amplitudes of the THz radiation is plotted for the frequencies of the first- and the second-order plasmons. The photon energy is given in terms of an excess energy of the photogenerated charge carriers (excess energy: photon energy minus band-gap energy of bulk GaAs of 1.515 eV). The amplitude of the THz radiation rises strongly above the GaAs band gap but flattens at an excess energy of 50 meV. For higher excess energy, the amplitude rises again. Comparing these data with the band diagram displayed in Fig. 1, one is led to conclude that the rise of the THz signal up to an excess

energy of 50 meV is much better explained by absorption into the quantized conduction-band states of the accumulation layer than by absorption in bulk GaAs. Note that optical transitions into the quantized states of the accumulation layer exhibit a much broader absorption edge than do interband transitions in compositional quantum wells. This results from the lack of confinement, and hence of quantization, of the valence-band states. For interband transitions into each electronic state in an accumulation layer, one expects an onset of absorption already at the band gap of bulk GaAs and a strong rise of absorption above the Fermi level up to an excess energy corresponding to the excitation from the lowest valence-band position into the E_0 energy eigenstate.²⁷ The rise shown in Fig. 6 of the THz-radiation amplitude reflects this absorption behavior expected for optical transitions within an accumulation layer.

In contrast to the experiments reported in Ref. 3, the plasmons observed in our experiments are coherent, i.e., phase synchronous relative to each other and to the optical excitation pulse. This imposes the additional requirement on the plasmon generation process that the energy redistribution driving the plasmon oscillations must occur on a time scale faster or equal to a quarter of the plasma oscillation period. For the rather high carrier density of the background plasma ($N_s = 5 \times 10^{11} \text{ cm}^{-2}$),

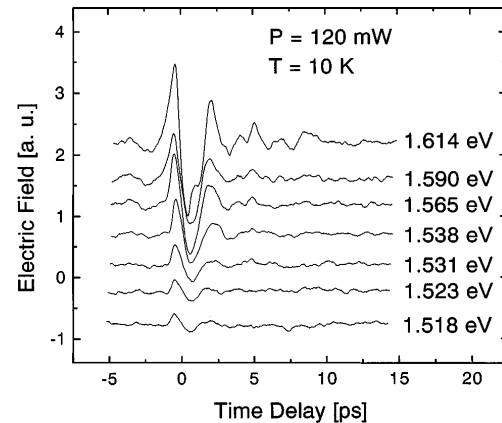


Fig. 4. Dependence of the emitted THz radiation on the energy of the optical excitation beam.

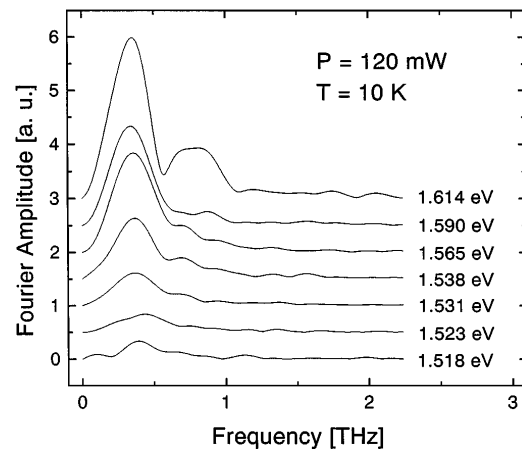


Fig. 5. Dependence of the emitted THz radiation on the photon energy of the optical excitation beam. The Fourier transforms of the time-domain data of Fig. 4 are displayed.

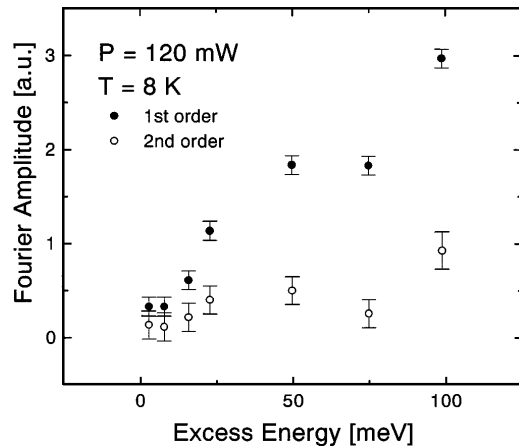


Fig. 6. Amplitude of the emitted THz radiation as a function of the excess energy per photogenerated electron–hole pair. The error bars result from the special Fourier procedure.

one expects redistribution of the optically deposited excess energy among the charge carriers of the 2DEG to take place on a 100-fs time scale.²⁸

In the cw FIR emission studies of Ref. 3 with current-mediated excitation of plasmons, the emission intensity was found to have the temperature dependence of a Bose–Einstein distribution with a temperature equal to that of the 2DEG. It was concluded that single-particle and collective excitations by the dc current are in thermal quasi-equilibrium with each other and that the FIR emission is essentially thermal radiation with a spectrum composed of contributions from the free-carrier and the plasmon excitations. The temperature of the electrons is determined by the applied electrical current.

In our experiments plasmon generation may also proceed by means of energy transfer into the 2DEG in analogy to the experiments of Ref. 3, but with optical instead of electrical energy deposition. Assuming thermal equilibrium, for the sake of argument, one estimates that the photogeneration of 1.5×10^{10} electron–hole pairs/cm² initially excited with an excess energy of 130 meV heats the 2DEG by 23 K. This temperature rise is comparable with the carrier heating held responsible in Ref. 3 for the dc-current-mediated excitation of radiative plasmon modes. In contrast to these experiments, the initial energy transfer in our experiments occurs locally, in the open areas of the grating. This spatially modulated heating induces some selectivity into the excitation of plasmon modes.

In contrast to this thermalization model of plasma generation, another mechanism based on local currents is feasible. The metallic grating acts as a mask at the illumination of the sample with the laser beam. The resulting lateral modulation of the density of photoexcited electrons can drive local currents from the high-density regions between the grating lines to the low-density regions beneath them. These currents are expected to drive plasma oscillations.

So far, we have neglected symmetry aspects of plasmon generation. Both excitation processes drive plasmon modes propagating in either of the two directions perpendicular to the grating lines. Under normal incidence the amplitudes of the counterpropagating plasmons are equal. The superposition of plasmons of the same order, but of

the opposite propagating direction, results in a standing wave that is not associated with a net dipole moment and hence does not emit radiation. The oblique incidence of the optical excitation pulse in our experiments causes an asymmetry of the distribution of the photoexcited charge carriers. The edges of the grating lines and the semiconductor underneath are illuminated on the side exposed to the optical beam but not on the other side. Because of this asymmetry in the excitation conditions, plasmon modes of opposite momentum are not excited with equal amplitude. A net dipole moment and emission of THz radiation are expected.

We can experimentally verify that the asymmetry of illumination is crucial for the THz-emission results by changing the angle of incidence of the optical beam. We have performed room- and low-temperature experiments in which the sample is rotated. When the angle of incidence is changed from 45° to normal, the THz radiation disappears. The effect cannot be explained by the orientation of the dipoles associated with plasmon oscillations. The dipole axes are parallel to the surface, and hence optimum emission by individual dipoles is expected normal to the surface.

The experimental data do not allow us to decide whether one of the two excitation mechanisms, the energy transfer or the transport process, is more important than the other. It is likely that an interplay of both processes has to be considered for the generation of coherent plasmons in our experiments.

C. Temperature Dependence

Having addressed possible plasmon generation mechanisms, we concentrate below on the phenomenology of the signal decay. The decrease of the coherent THz radiation with time can originate either from the loss of coherence within the ensemble of photoexcited plasmons (dephasing) or from the reduction of the total number of plasmons by decay processes. Our experiments do not allow us to distinguish between these two signal decay mechanisms.

In the low-temperature data presented so far, THz emission by coherent plasmons has a duration of the order of 3 ps. To investigate the temperature dependence of the decay time, we perform THz-emission measurements at various sample temperatures. THz transients,

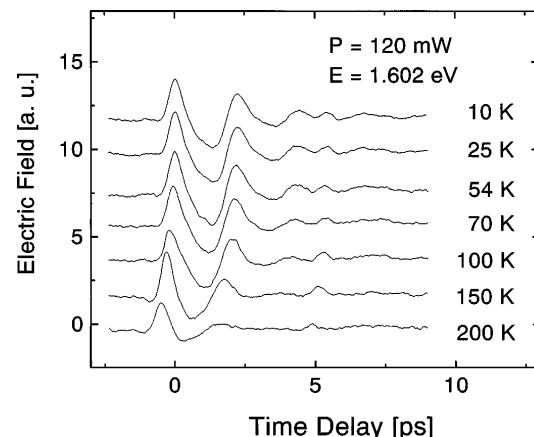


Fig. 7. Temperature dependence of the waveform of the coherent THz radiation from 2D plasmons excited by optical pulses with a photon energy of 1.602 eV.

measured at an excitation photon energy of 1.602 eV, are shown in Fig. 7. From room temperature (data not shown) to as low as 200 K, the THz waveform consists of only a single-cycle oscillation. The small peak at 5.5 ps after the main pulse is the residual reflection from the wafer's back side. With decreasing temperature the single-cycle oscillation develops into an oscillation consisting of several periods. Figure 8 shows the Fourier transforms of Fig. 7. At 200 K the emission spectrum is broad, with a maximum at 0.45 THz. A second peak at 0.9 THz appears in the high-frequency shoulder of the main peak when the temperature is reduced to 150 K. The peak frequencies of these oscillations correspond well with the calculated frequencies of the first- and the second-order radiative plasmon modes.

To determine the decay time (or, correspondingly, the linewidth) of the coherent plasmon modes, the residual reflected pulse from the time-domain data is removed by numerical subtraction without compromising the bandwidth information. This is accomplished by subtraction of a time-shifted and amplitude-adjusted replica of the initial part of the signal. The procedure relies on the observation that the reflected pulse does not suffer significant distortion during propagation through the sample. After numerical removal of the reflected signal and Fourier transformation of the time-domain data, the spectra are corrected for the spectral sensitivity of the measurement system. The plasmon resonances at 0.45 and 0.9 THz are then fitted with Lorentzians, assuming homogeneous line broadening. Figure 9 illustrates the fitting procedure in an exemplary way for the 10 K data presented in Fig. 8. The measured spectrum (dotted curve) is sensitivity corrected. The spectral function of the detection system as determined by control measurements with an InP surface emitter is shown in the inset of Fig. 9. In such measurements THz radiation is emitted off the depletion region at the surface of an InP:Fe wafer, yielding a quasi-white-light spectrum in the THz regime useful for calibration of the system.²⁹ In the modeling process of the corrected plasmon emission data, the Lorentzian function for the first-order plasmon peak at 0.45 THz is adjusted to the high-frequency side of the line because one observes an unexplained asymmetric line shape of this resonance in all the corrected spectra. The two depicted Lorentzian functions for the first- and the second-order plasmon resonances reproduce the measured line shapes rather well.

Figure 10 displays the width γ of the first- and the second-order plasmon emission lines obtained by the fitting procedure. The error bars result from the uncertainties in the Fourier transform and the fitting procedure but do not affect the mean results. The corresponding amplitude decay time $\tau = 1/(\pi\gamma)$ is also plotted in Fig. 10. The linewidths of the two peaks are indistinguishable within the limits of the fit and show the same temperature dependence. From 200 to 10 K the linewidths decrease from 0.27 THz ($\tau = 1.2$ ps) to 0.11 THz ($\tau = 2.9$ ps), with a rapid decrease down to 100 K followed by a much more gradual decrease from 100 to 10 K.

The sample-temperature dependence of the amplitude decay time τ above 100 K is explained by scattering of the plasmons with optical phonons. Below 100 K, the optical-phonon population is too low to be the limiting

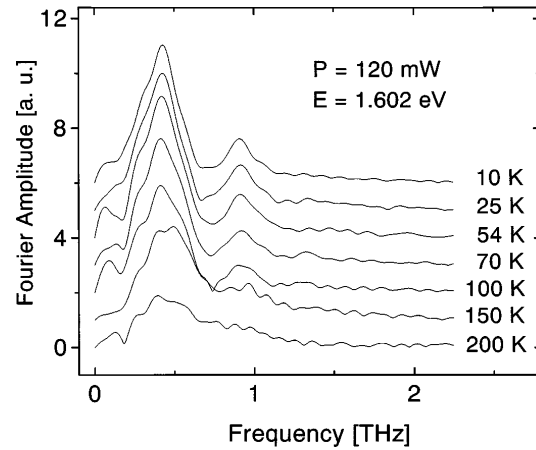


Fig. 8. Temperature dependence of the coherent THz radiation from plasmons. The Fourier transforms of the time-domain data of Fig. 7 are shown.

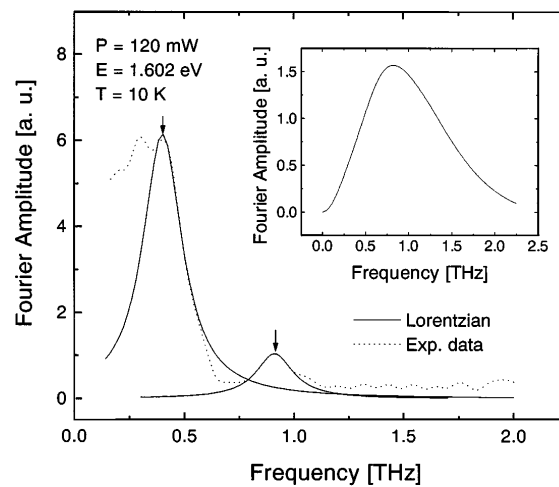


Fig. 9. Illustration of the fitting procedure. The figure displays the spectrum of the 10 K curve shown in Fig. 5, corrected for the sensitivity of the detection system. The Lorentzian-fitted curves for the first- and the second-order plasmon resonance are marked with arrows. In the inset the spectral response of the detection system is displayed. P, excitation power; E, photon energy; T, sample temperature.

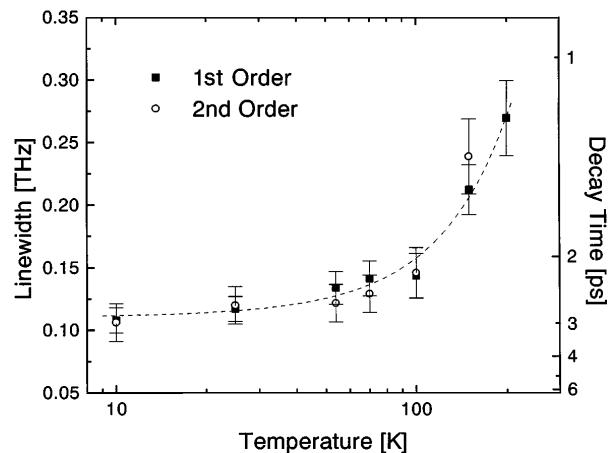


Fig. 10. Linewidth and corresponding decay time of the plasmon emission peaks as a function of temperature. The error bars reflect the uncertainties of the fitting procedure. The dashed curve is a guide for the eye.

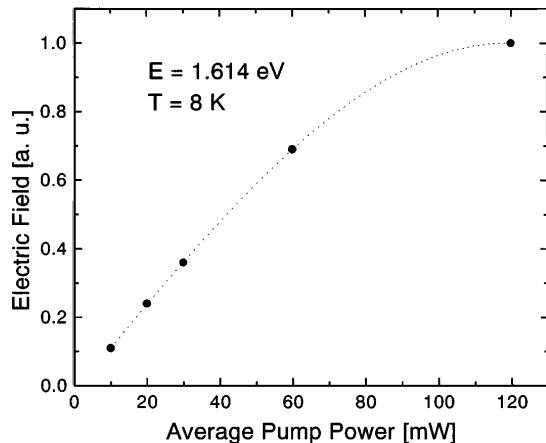


Fig. 11. Amplitude of the emitted THz radiation as a function of the average power of the optical pump beam.

factor for plasmon dephasing or decay. In this temperature regime other dephasing or decay processes are relevant. As discussed in detail in Subsection 5.B, additional scattering mechanisms of the coherent plasmons with electrons, holes, and noncoherent plasmon modes are considered.

D. Pump Power and Emitted Power

Experiments in which the power of the excitation beam is varied to yield information about the dependence of the plasmon decay time on the electron-hole density are the focus of this subsection. Figure 11 presents the dependence of the THz-signal amplitude on the average power of the optical pump beam (photon energy, 1.614 eV; sample temperature, 8 K). The amplitude rises linearly with pump power up to 60-mW average power. Above this level, however, the THz amplitude begins to saturate. The linear rise is consistent with the superradiant nature of the emission process. The power of the radiation emitted from a coherent ensemble of dipoles is expected to depend quadratically on the number of cooperatively emitting dipoles (which is proportional to the number of excited radiative plasmons).^{30,31} Hence the THz amplitude should exhibit a linear dependence on the pump power, as is indeed observed in the experiment for low optical pump powers. The saturation at high pump power is not understood at present. Saturation is expected when the density of the photogenerated carriers approaches that of the background plasma. However, even at a power as high as 120 mW, the density of photogenerated electron-hole pairs in the accumulation layer does not exceed $2 \times 10^{10} \text{ cm}^{-2}$, a value $25\times$ smaller than that of the carrier density of the background plasma. Screening effects are also insignificant. This is corroborated by the observation that the decay-time constant of the THz radiation does not change up to the highest pump powers of the experiment (data not shown).

The average power of the THz radiation itself is difficult to determine in absolute units, as we do not have a calibrated and sufficiently sensitive power meter for the THz frequency range available. We can resort, however, to the following comparative procedure. Measuring the amplitude of THz radiation from bulk InP:Fe surface emitters,²⁵ which are often applied as standard sources

for THz pulses, we find that the peak field amplitude of the radiation from plasmons is approximately a factor of 10 smaller for the same optical pump power and the same photon energy of 1.602 eV. This ratio can be converted into absolute power units, as the average power of the THz pulses from InP surfaces is evaluated following the method of Ref. 32 to be 3 nW at an optical beam power of 100 mW. Although the radiation intensity from plasmons is 100 times lower, the emission efficiency is remarkably high when calibrated with the absorption in the accumulation channel. A large part of the incident light is reflected off the grating, and only 1% of the incident optical power is absorbed in the accumulation region. Taking into consideration that the THz intensity scales quadratically with the absorbed optical beam power, we would expect the intensity of the THz radiation from plasmons to be 100 times higher than for InP:Fe surface emitters if the incident light were absorbed entirely at the AlGaAs/GaAs interface.

5. DISCUSSION

A. Plasmon Generation Mechanism

Having discussed the fact that excitation of coherent plasma oscillations may proceed by ultrafast thermalization processes or current surges, we address the possibility of plasmon excitation by means of single-electron relaxation processes. We show that, for a 2DEG with and without a grating coupler, the simultaneous requirements of conservation of momentum and of energy during such a scattering event rule out single-particle scattering as the origin of plasma oscillations under the conditions of our experiments. We further show that the presence of the grating imposes an additional selection rule forbidding plasmon emission by single electrons.

Relaxation of excited electrons by the emission of plasmons is the reverse of Landau damping, the decay of plasmons into single-electron excitations. Figure 12 displays the Fermi sphere of the 2DEG. On optical excitation, additional electrons are excited into the conduction band. Assuming monoenergetic excitation (for simplicity), the photogenerated electrons are found on a sphere in k_x, k_y space (with x, y denoting orthogonal directions within the plane of the 2DEG). If an electron is to emit a plasmon during a scattering process, energy- and momentum-conservation laws have to be obeyed. The electron scatters from a state \mathbf{k} to a state $\mathbf{k}' = \mathbf{k} - \mathbf{q}$, with \mathbf{k} and \mathbf{k}' being the wave vector of the electron before and after the scattering process, respectively, and \mathbf{q} being that of the generated plasmon. Energy conservation requires that the final states are located on a sphere centered at the origin of k_x, k_y space with a radius given by $\hbar^2 k'^2/2m^* = \hbar^2 k^2/2m^* - \hbar\omega_{\text{pl}}$. $\hbar\omega_{\text{pl}}$ is the plasmon energy. Considering the selection rules for momentum and energy, the emission of a plasmon leads to the following condition:

$$\frac{\hbar k}{m^*} > \frac{\omega_{\text{pl}}}{q} \quad (4)$$

under the assumption that $q \ll k$, which is generally fulfilled. In a more physical picture, the velocity of the electrons v_{kin} must exceed the phase velocity v_{pl} of the plasmons ($v_{\text{kin}} > v_{\text{pl}}$).

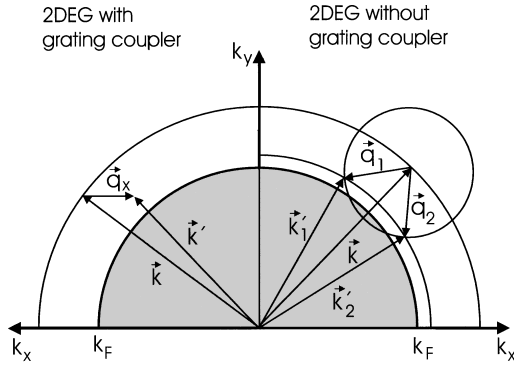


Fig. 12. K -space illustration of the energy- and momentum-conservation laws for the emission of a plasmon by scattering processes with single electrons. Without a grating coupler on the sample surface (right-hand side), plasmons with \mathbf{q} -vector components in the \mathbf{q}_x and the \mathbf{q}_y directions can be generated. With a grating coupler with the metal lines parallel to the y direction (left-hand side), the q_y component of the plasmon wave vector has to vanish. This restriction considerably limits the number of permitted relaxation channels.

On the right-hand side of Fig. 12, the situation of a heterointerface without a grating coupler is depicted. According to relation 4, the number of possible final states for the electron is 0, 1, or 2, depending on the values of k and q . An example of a heterojunction with the parameters of our experiments, but without a metal grating, is as follows: one calculates for an electron excess energy of 100 meV that plasmons with frequencies $\nu_{\text{pl}} > 2.2$ THz fulfill the condition of relation 4 but that plasmons with lower frequencies cannot be excited by single-electron relaxation.

For a grating-coupled 2DEG, an additional selection rule has to be considered. The left-hand side of Fig. 12 shows the conditions for a heterointerface with a grating coupler. Assuming that the grating lines are parallel to the y axis, \mathbf{q} has only a \mathbf{q}_x component. As mentioned above, this additional selection rule reflects that plasmon propagation is limited to the x direction. Plasmons with a \mathbf{q}_y wave-vector component would have an oscillating electric-field component along the grating lines. This field component is suppressed by the induced screening currents in the grating, which has a very high (ideally, an infinitely large) conductivity in the x direction.²³ This selection rule has a drastic influence on the scattering channels available for plasmon emission by an electron. Except for very specific momenta \mathbf{k} and \mathbf{q}_x , both momentum and energy conservation cannot be fulfilled simultaneously. For all practical purposes, plasmon generation by single-electron relaxation is forbidden.

Nevertheless, it is interesting to check relation 4, $v_{\text{kin}} > v_{\text{pl}}$, for the sample parameters of our experiment. One obtains the following values: $v_{\text{kin}} = 3 \times 10^5$ m/s for an electron with the quasi-Fermi energy of 18 meV and $v_{\text{kin}} = 7 \times 10^5$ m/s for an excess energy of 100 meV, respectively. The phase velocity for a first-order (third-order) plasmon is calculated to be $v_{\text{pl}} = 1.5 \times 10^6$ m/s (1.3×10^6 m/s). Thus the condition $v_{\text{kin}} > v_{\text{pl}}$ is not fulfilled, and relation 4 provides another reason that single-electron relaxation cannot be relevant under the present experimental conditions (excess energy and sample parameters).

One has to invoke more-complex processes for the generation of coherent plasmons. An analysis of such processes is well beyond the scope of this paper.

B. Low-Temperature Plasmon Decay

We now address the low-temperature decay rate of the radiative plasmon modes displayed in Fig. 10 and discuss mechanisms responsible for the decay.

Let us first point out that the carrier-plasmon interactions that are responsible for plasmon generation may also lead to plasmon dephasing or, correspondingly, to decay. In this regard, it is surprising that we observe experimentally a low-temperature dephasing or decay time 3 ps, much longer than the time permitted for plasmon generation (approximately 1/4 oscillation period). This observation suggests that the relevant carrier-plasmon interactions are most effective immediately after optical excitation but lose efficiency as time progresses. The decline in carrier-plasmon coupling efficiency should be associated with the relaxation of the optically excited electrons and their becoming a part of the 2DEG.

The low-temperature decay time τ of 3 ps at temperatures below 100 K is significantly longer than that of optically excited coherent plasmons recently observed in a three-dimensional (3D) electron-hole gas in GaAs ($\tau = 0.3\text{--}0.5$ ps for carrier-pair densities of 1.1×10^{16} cm³ to 0.2×10^{16} cm³).³³ The faster decay in the 3D case may be explained by Landau damping, which is permitted in the 3D case but is not effective in the 2D system investigated here because of the same considerations presented above in the context of single-electron relaxation. If we follow the same line of argumentation as above, it is obvious that Landau damping is important only for high-frequency plasmons ($\nu_{\text{pl}} > 2.2$ THz) in a 2DEG without a grating coupler and that it is completely ineffectual in a 2DEG with a grating coupler.

The low-temperature decay-time constant in our measurements is significantly shorter than the decay time of the dc-current-induced plasma oscillations investigated in Ref. 3. There the decay-time constant was inferred from the plasmon resonances in the cw FIR emission spectra. The observed linewidth of 0.45 meV yielded an effective linewidth of 0.1 meV after deconvolution with the detection bandwidth (0.35 meV). It was concluded that the effective linewidth is dominated by the intrinsic single-particle momentum-scattering time that was determined from magnetotransport data to be 16 ps.

The shorter decay time of our experiments is certainly not an artifact of bandwidth limitations because the bandwidth in our measurements is determined by the time window applied in the Fourier analysis of the time-domain data. With an analysis as illustrated in Fig. 9, the intrinsic linewidth of the radiative plasmon resonances is determined.

Although the precise origin of the faster decay of the optically excited 2D plasmons is not clear at present, several factors discussed below are likely to contribute. The faster decay may be a consequence of more efficient single-particle interactions and of a nonequilibrium character of the excited plasmon modes. (i) Single-particle interactions may be more significant than in the cw FIR measurements for two reasons. First, the photogeneration of electron-hole pairs introduces holes into the accumu-

lation channel that are not present in the experiments of Ref. 3. Interaction between electrons or plasmons with holes provides an additional relaxation channel to be considered. Second, one has to take into account additional carrier heating effects that do not exist in the cw measurements. Electrons that are photoexcited at the edge or away from the accumulation channel and experience the influence of the space-charge field will be transferred into the channel. The excess energy that they acquire during this vertical transport contributes to a rather persistent heating of the electrons in the channel. Plasmons generated by this energy transfer are out of phase with the initially excited plasmons. They do not contribute to the coherent THz radiation but rather represent additional scatterers for the coherent plasmons. (ii) The faster decay may also reflect a strong nonequilibrium character of the excited coherent plasmon modes. Efficient coupling to cold modes as well as to strongly excited nonradiative modes may lead to a stronger plasmon interaction and to a faster decay than in the cw FIR measurements.

6. CONCLUSION

In summary, we have presented the first observation of the emission of electromagnetic radiation from optically excited coherent plasma oscillations in a two-dimensional electron gas at an AlGaAs/GaAs heterojunction. THz-emission spectroscopy permits the direct detection of the coherent radiation field. Plasmon generation appears to occur by means of surge currents in combination with ultrafast thermalization processes, although plasmon excitation by single-particle scattering events can be ruled out as the driving mechanism. The decay of the coherent THz signal at temperatures above 100 K is determined by plasmon scattering with optical phonons. Below 100 K, the THz signal decays considerably faster than does the FIR radiation detected in transport measurements, indicating that optical excitation induces additional relaxation channels for the plasmons.

ACKNOWLEDGMENTS

The research at Aachen was supported by the Deutsche Forschungsgemeinschaft and the Alfried Krupp Foundation. The research at the University of Tokyo was sponsored by a Grant-in-Aid from Japan's Ministry of Education, Science, and Culture and by the Industry-University Joint Research Program Quantum Nanoelectronics.

*E-mail address, roskos@zyklop.basl.rwth-aachen.de.

REFERENCES AND NOTES

- G. Schedelbeck, R. Strenz, G. Abstreiter, G. Böhm, and G. Weimann, *Solid State Commun.* **93**, 569 (1995).
- R. Höpfel, G. Lindemann, E. Gornik, G. Stangl, A. C. Gossard, and W. Wiegmann, *Surf. Sci.* **113**, 118 (1982).
- K. Hirakawa, K. Yamanaka, M. Grayson, and D. C. Tsui, *Appl. Phys. Lett.* **67**, 2326 (1995).
- D. C. Tsui, E. Gornik, and R. A. Logan, *Solid State Commun.* **35**, 875 (1980).
- R. A. Höpfel, E. Vass, and E. Gornik, *Phys. Rev. Lett.* **49**, 1667 (1982).
- S. J. Allen, Jr., D. C. Tsui, and R. A. Logan, *Phys. Rev. Lett.* **38**, 980 (1977).
- T. N. Theis, J. P. Kotthaus, and P. J. Stiles, *Solid State Commun.* **26**, 603 (1978).
- E. Batke, D. Heitmann, J. P. Kotthaus, and K. Ploog, *Rev. Lett.* **54**, 2367 (1985).
- D. Olego, A. Pinczuk, A. C. Gossard, and W. Wiegmann, *Phys. Rev. B* **25**, 7867 (1982).
- H. G. Roskos, M. C. Nuss, J. Shah, K. Leo, D. A. B. Miller, A. M. Fox, S. Schmitt-Rink, and K. Köhler, *Phys. Rev. Lett.* **68**, 2216 (1992).
- C. Waschke, H. G. Roskos, R. Schwedler, K. Leo, H. Kurz, and K. Köhler, *Phys. Rev. Lett.* **70**, 3319 (1993).
- H. G. Roskos, in *Festkörperprobleme/Advances in Solid State Physics*, R. Helbig, ed. (Vieweg Verlag, Braunschweig, Germany, 1994), Vol. 34, p. 297.
- K. Hirakawa, M. Grayson, D. C. Tsui, and Ç. Kurdak, *Phys. Rev. B* **47**, 16651 (1993).
- T. Ando, *J. Phys. Soc. Jpn.* **51**, 3893 (1982).
- F. Stern, *Phys. Rev. Lett.* **18**, 546 (1967).
- C. D. Ager, R. J. Wilkinson, and H. P. Hughes, *J. Appl. Phys.* **71**, 1322 (1992).
- C. D. Ager and H. P. Hughes, *Solid State Commun.* **83**, 627 (1992).
- C. D. Ager and H. P. Hughes, *Phys. Rev. B* **44**, 13452 (1991).
- M. V. Krasheninnikov and A. V. Chaplik, *Sov. Phys. Semicond.* **15**, 19 (1981).
- R. E. Tyson, D. E. Bangert, and H. P. Hughes, *J. Appl. Phys.* **76**, 5909 (1994).
- N. Okisu, Y. Sambe, and T. Kobayashi, *Appl. Phys. Lett.* **48**, 776 (1986).
- R. Poerschke, ed., *Data in Science and Technology, Semiconductors, Group IV Elements and III-V Compounds*, (Springer-Verlag, Berlin, 1991).
- L. Zheng, W. L. Schaich, and A. H. MacDonald, *Phys. Rev. B* **41**, 8493 (1990).
- The orientation of the grating lines with respect to the plane of incidence is of significance only for the excitation intensity, but not for the THz-emission results discussed here. We have experimentally verified that the relevant features of the THz data are reproduced when the angle of incidence is changed from perpendicular to parallel.
- X.-C. Zhang, B. B. Hu, J. T. Darrow, and D. H. Auston, *Appl. Phys. Lett.* **56**, 1011 (1990).
- N. M. Froberg, B. B. Hu, X.-C. Zhang, and D. H. Auston, *IEEE J. Quantum Electron.* **28**, 2291 (1992).
- E. S. Snow, O. J. Glembocki, and B. V. Shanabrook, *Phys. Rev. B* **38**, 12483 (1988).
- J. A. Kash, *Phys. Rev. B* **48**, 18336 (1993).
- T. Dekorsy, H. Auer, H. G. Roskos, and H. Kurz, "THz electromagnetic emission by coherent infrared active phonons" *Phys. Rev. B* (to be published).
- R. H. Dicke, *Phys. Rev.* **93**, 99 (1953).
- K. Victor, H. G. Roskos, and C. Waschke, *J. Opt. Soc. Am. B* **11**, 2470 (1994).
- M. van Exter and D. Grischkowsky, *IEEE Trans. Microwave Theory Tech.* **38**, 1684 (1990).
- W. Sha, A. Smirl, and W. F. Tseng, *Phys. Rev. Lett.* **74**, 4273 (1995).